Available online at www.sciencedirect.com
ScienceDirect
Journal of Power Sources 170 (2007) 268–274
JOURNAL OF POWER SOURCES
www.elsevier.com/locate/jpowsour

Thermal nitridation of chromium electroplated AISI316L stainless steel for polymer electrolyte membrane fuel cell bipolar plate

Dae-Geun Nam [a,b,*], Hu-Chul Lee [b]

[a] *R&D Center, Rotem Company, Uiwang 437-718, Republic of Korea*
[b] *School of Materials Science and Engineering, Seoul National University, Seoul 151-744, Republic of Korea*

Received 23 February 2007; received in revised form 12 April 2007; accepted 19 April 2007
Available online 27 April 2007

Abstract

The electrical and corrosion properties of surface-nitrided AISI316L stainless steel are evaluated to assess the potential use of this material as a bipolar plate for a polymer electrolyte membrane fuel cell. Chromium is electroplated on the surface of the AISI316L stainless steel before nitridation. The nitriding condition is selected so as to form Cr_2N nitride only and the result is compared with that of a $CrN + Cr_2N$ nitride coating. The stainless steels with the Cr_2N nitride protective coating layer exhibit better interfacial contact resistance and corrosion resistance than the as-rolled or ($CrN + Cr_2N$)-coated AISI316L stainless steels.

Keywords: Fuel cell; Bipolar plate; Chromium nitride; Stainless steel; Corrosion resistance; Interfacial contact resistance

1. Introduction

Fuel cells are electrochemical devices that convert the chemical energy of a reaction directly into electrical energy [1]. The polymer electrolyte membrane fuel cell (PEMFC) is one of the most promising candidates for vehicular power sources and for domestic combined heat and power (CHP) systems. The PEMFC operates at low temperature (60–80 °C) and has a high specific power and compactness. Nevertheless, its high cost and poor system durability hinder its commercial application. The bipolar plate is one of the most important components of the PEMFC, and amounts to nearly 80% of the weight and nearly 40% of the cost of the total stack [2]. In spite of its poor mechanical properties and high cost, graphite has been most widely used as a bipolar plate material. To reduce the cost and weight of PEMFCs, metallic bipolar plates have been very much sought after as an alternative. Stainless steels, which have good mechanical properties and relatively low cost, would be good candidate materials for metallic bipolar plates [3], but a passive film is formed on their surface. This film is good for their corrosion resistance during PEMFC operation but has high electrical resistivity and increases the interfacial contact resistance (ICR) between the bipolar plate and electrode. Methods for improving the ICR as well as the corrosion resistance of metallic bipolar plates have been actively researched. Protective layers such as transition metal nitrides have been suggested as promising coating materials. The thermal nitridation of stainless steels or high chromium alloys has been attempted to improve the surface properties of bipolar plates [4–7]. To form a continuous chromium nitrided layer, the chromium content in the substrate should be as high as 50%, which incurs a high alloy cost. Chromium electroplating is a cost-effective way to increase the chromium content on the surface of stainless steels. Thermal nitridation of chromium can lead to the formation of two types of chromium nitride, CrN and Cr_2N, and the resulting thermally grown chromium nitrided layer consists of a surface layer of CrN on top of a Cr_2N layer [4,8]. The electrical resistivity of CrN is very high, i.e., 600–800 μΩ cm, compared with that of Cr_2N, which is only 79–89 μΩ cm [9]. Therefore, removal of the CrN layer would reduce the surface electrical resistance of the nitrided layer.

In this study, the nitridation conditions for the growth of Cr_2N nitride are evaluated thermodynamically and the interfacial contact resistance and corrosion resistance of the thermally grown Cr_2N layer on the surface of Cr electroplated AISI316L stainless steel are evaluated for use of this material as PEMFC bipolar plates.

* Corresponding author. Tel.: +82 31 460 1929; fax: +82 31 460 1782.
E-mail addresses: trinad@rotem.co.kr, trinad@nate.com (D.-G. Nam).

0378-7753/$ – see front matter © 2007 Elsevier B.V. All rights reserved.
doi:10.1016/j.jpowsour.2007.04.054

2. Experimental

2.1. Material and surface treatment

AISI316L stainless-steel sheets with a thickness of 2 mm were used as the substrates. The chemical composition (in wt.%) of the steel is 0.019C, 0.52Si, 1.49Mn, 0.025P, 0.002S, 16.9Cr, 11.1Ni, 2.06Mo, and the balance Fe. The surface of each sheet was polished with #600 grit SiC paper and degreased with acetone in an ultrasonic cleaner. Conventional nickel strike was applied to the polished surface for the purpose of surface activation. Chromium electroplating was performed in a Sargent bath that contained 150 g dm^{-3} CrO_3 and 1 g dm^{-3} H_2SO_4 in distilled water [10]. Nitriding was performed for 2 h at 1100 °C in a furnace with a controlled nitrogen partial pressure. The nitrogen gas pressure was set to 100 Torr or 1 atm according to the thermodynamic calculations. The specimens were cut into discs of 1 cm diameter and the untreated surface was polished with #600 grit SiC paper.

2.2. Thermodynamic calculation

The nitridation conditions for the growth of the CrN and Cr_2N nitrides from the electroplated chromium layer were evaluated [11]. Thermo-Calc Version Q software was used in the thermodynamic calculation of the Gibbs free energy for the formation of CrN and Cr_2N chromium nitrides from 1 mol of chromium with the database, SUB97 [12].

2.3. Microstructure and X-ray diffraction

The planar and cross-sectional microstructures of the chromium electroplated and thermally nitrided layers of stainless steels were observed by means of a JEOL JSM-5600 scanning electron microscope (SEM). The crystal structure of the nitrided layers was investigated by means of a MAC Science M18XHF-SRA X-ray diffractometer (XRD). A Cu Kα source was used for the XRD measurements at a scanning rate of 5° min^{-1}.

2.4. Interfacial contact resistance

The ICR of the surface nitride stainless steel was measured at room temperature by a method similar to that proposed by Wang et al. [3] and Davies et al. [13] with an Instek GOM-802 milliohm meter. A schematic diagram of the set-up used for the ICR measurement is shown in Fig. 1. Toray TP-060S carbon paper was used and strengthened copper chromium alloy was employed for the copper jigs shown in Fig. 1. The ICR value, the resistance of the carbon paper and nitrided layer interface ($R_{(2)}$), was obtained by subtracting the separately measure value of $R_{(1)+(3)+(4)}$ from the measured total resistance, $R_{(1)+(2)+(3)+(4)}$. The resistance of the two carbon paper/copper alloy jig interfaces ($R_{(1)+(4)}$) for each compaction force can be measured by placing a carbon paper between the two jigs. The resistance of the carbon paper/substrate interface ($R_{(3)}$) can be measured by putting an untreated substrate between the two carbon papers. Considering

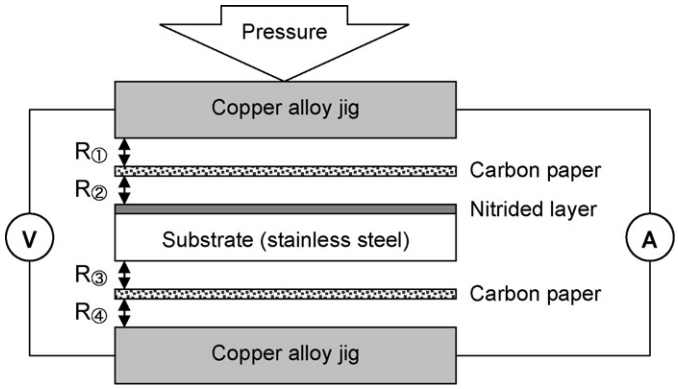

Fig. 1. Schematic diagram of the measurement of the interfacial contact resistance.

the conventional packing load for the stack (100–150 N cm^{-2}), the compaction force used for the ICR measurements was varied up to 150 N cm^{-2}.

2.5. Corrosion resistance

Bipolar plates are used in a very corrosive environment. For the corrosion tests, 1 M H_2SO_4 + 2 ppm F^- solution at 80 °C was used to simulate the internal operating conditions of PEMFC stacks [14]. A three-electrode system was used, in which a saturated calomel electrode (SCE) served as the reference electrode, a platinum sheet as the counter electrode, and a rotating disc electrode (RDE) with a nitrided stainless steel as the counter electrode. The rotation speed of the RDE was 500 rpm and the RDE was stabilized for 5 min before the test. The potential was changed from the open-circuit potential (OCP) to 1.2 V at a scanning rate of 5 mV s^{-1}. An EG&G Potentiostat/Galvanostat Model 273 controlled by M352 corrosion software was employed for the measurement. The current densities at an anode potential of −0.1 V and a cathode potential of 0.6 V were adopted to characterize the electrochemical properties [15].

3. Results

3.1. Thermodynamic calculations

The Gibbs free energy for the formation of the chromium nitrides was calculated using Thermo-Calc version Q with the data base, SUB97 [12], as a function of the nitrogen partial pressure and temperature. In gas nitridation, CrN will form at a higher nitrogen partial pressure and at lower temperatures, while Cr_2N will be produced at a lower nitrogen partial pressure and at higher temperatures. The thermodynamically stable regions for Cr_2N and CrN nitrides are reconstructed in Fig. 2 as a function of the nitridation temperature and nitrogen partial pressure. For the conventional thermal nitriding condition with a nitrogen partial pressure of 1 atm (760 Torr) at 1100 °C, CrN is more stable and will grow first. At a nitrogen pressure of 100 Torr, however, Cr_2N nitride will form at 1100 °C. In the present experiments, nitrides were grown under

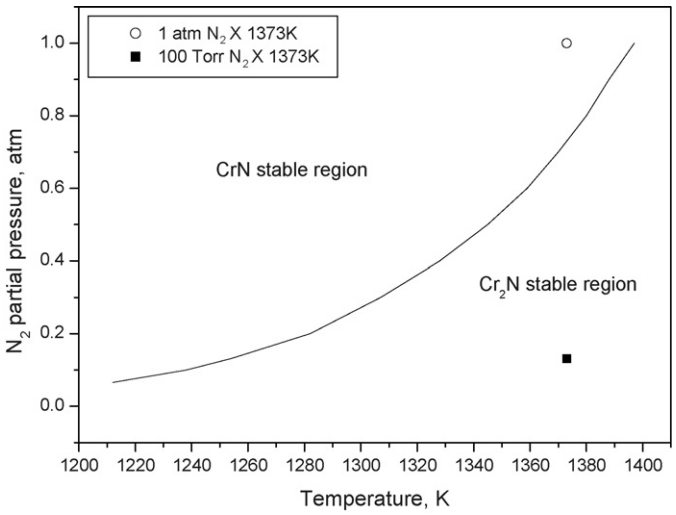

Fig. 2. Stable region of CrN and Cr_2N chromium nitrides calculated by Thermo-Calc version Q using the database, SUB97 [12].

both conditions and the surface electrochemical properties were compared.

3.2. Microstructural and X-ray diffraction analysis of chromium nitrided layer

Scanning electron micrographs of the electrodeposited chromium layer are shown in Fig. 3. Uniform growth of the chromium layer on the top of the nickel strike layer can be observed (Fig. 3(a)). Nickel strike activates the surface of the stainless steels and improves the throwing power of the chromium electroplating. Due to the strong tensile stresses that develop during electroplating, the electroplated chromium layer contains many cracks which extend from the nickel strike layer to the surface. A planar view of the electroplated chromium layer, is given in Fig. 3(b). This reveals the presence of many cracks. These cracks, which can cause crevice corrosion, should be eliminated.

The microstructures of the thermally nitrided chromium layer are presented in Fig. 4. The chromium nitrided layer is uniformly formed on the top of the surface of the stainless steel. Columnar growth of chromium nitride is observed below this uniformly grown nitrided layer (Fig. 4(a)). The nitrided layer is free from cracks. The cracks, which develop in the electroplated chromium layer, are all sealed off during growth of the nitride. Traces of sealed-off microcracks can be seen on the surface of the nitrided layer (Fig. 4(b)). No major defects are found in the chromium nitrided layer except for numerous isolated microvoids (Fig. 4(a) and (c)). These microvoids are believed to form during heating of the specimen to the nitriding temperature, because of the volume differences between amorphous and crystalline chromium.

The XRD patterns of electroplated chromium and the chromium nitrided layer formed at nitrogen partial pressures of 100 Torr and 1 atm are compared in Fig. 5. The diffraction peaks from the electroplated chromium layer are very weak, which suggests that most of this chromium layer is not crystalline. The XRD pattern from the nitrided layer formed at 1100 °C and a nitrogen pressure of 100 Torr shows diffraction peaks only from Cr_2N nitride, which corresponds with the result of the thermodynamic calculation. The XRD pattern from the nitrided layer formed at a nitrogen pressure of 1 atm shows diffraction peaks from CrN nitride as well as from Cr_2N nitride. According to the Thermo-Calc evaluation, CrN is expected to form at 1100 °C at a nitrogen pressure of 1 atm. Once the CrN layer forms on the top of the surface, however, it acts as a barrier to nitrogen diffusion and Cr_2N nitride grows below the CrN layer [16,17].

The electrical resistivity of CrN nitride is 600–800 μΩ cm, which is about eight times higher than that of Cr_2N nitride, viz., 79–89 μΩ cm [9]. By suppressing the formation of the CrN layer on the top of the nitrided layer, a reduction in the ICR of the bipolar plate can be expected.

According to the JCPDS data for Cr_2N [18], the peak intensity of the (3 0 0) plane is 15% of that of the (1 1 1) plane. The peak intensities of the (3 0 0) plane in Fig. 5 are 190% and 280% of those of the (1 1 1) plane for nitrogen pressures of 100 Torr and 1 atm, respectively. This means that the chromium nitrided layer is strongly textured. The mechanism of texture formation during the growth of the nitride is not yet clearly understood [16].

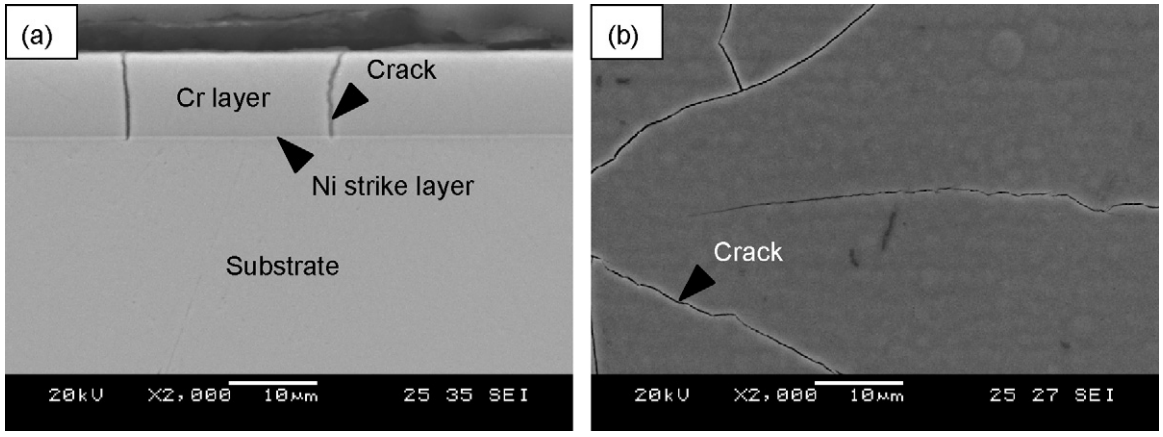

Fig. 3. SEM micrographs of (a) cross-section and (b) surface of Cr electroplated AISI316L stainless steel.

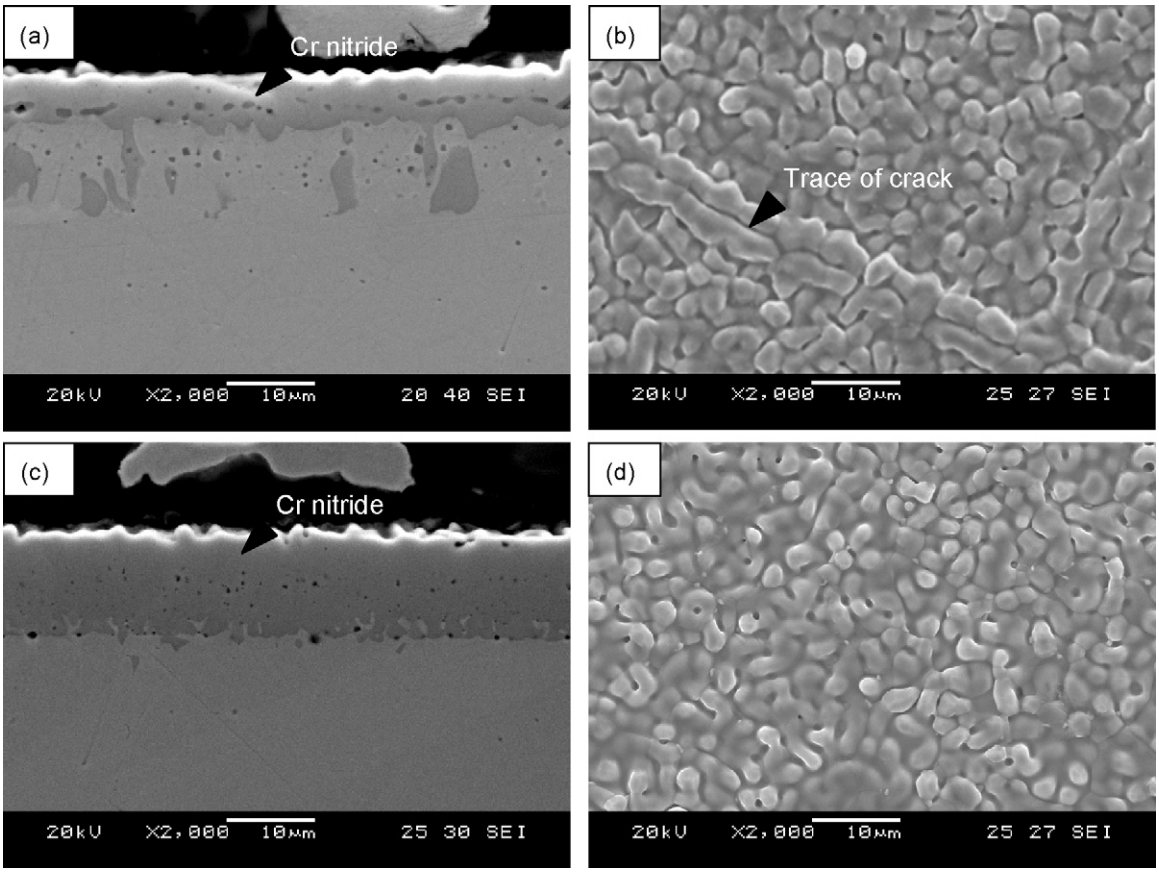

Fig. 4. SEM micrographs of the cross-section and surface of thermally nitrided AISI316L stainless steel (a and b) in 100 Torr N_2 (c and d) in 1 atm N_2.

3.3. Interfacial contact resistance

The results of ICR measurements on the chromium nitrided specimens are plotted in Fig. 6. The ICR data for bare AISI316L stainless steel and graphite are added for comparison. With increasing compaction force, the ICR decreases due to an increase in the contact area between the carbon paper and the specimen. The ICR values of the as-rolled, commercial, AISI316L stainless steel and graphite at a compaction force of 150 N cm^{-2} are 84 and 13 mΩ cm^2, respectively. At a low compaction force, the ICR values of the nitrided stainless steels are higher than that of bare AISI316L stainless steel, but become lower than that of bare AISI316L stainless steel when the compaction force is greater than 50 N cm^{-2}. This change may reflect

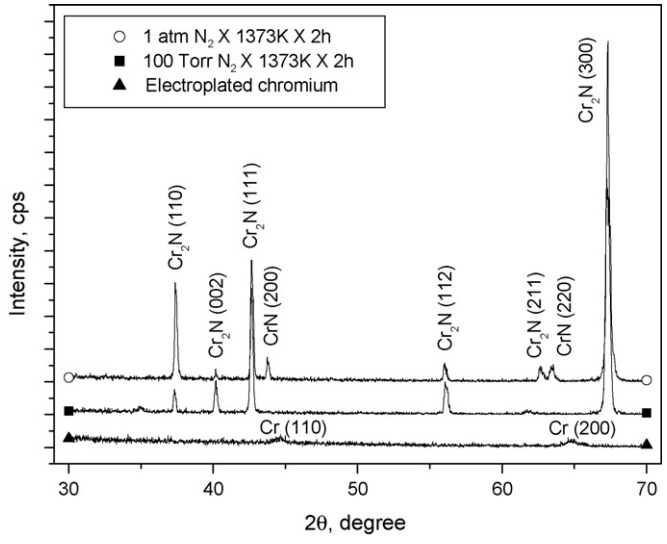

Fig. 5. XRD patterns of electroplated chromium and chromium nitrided layer.

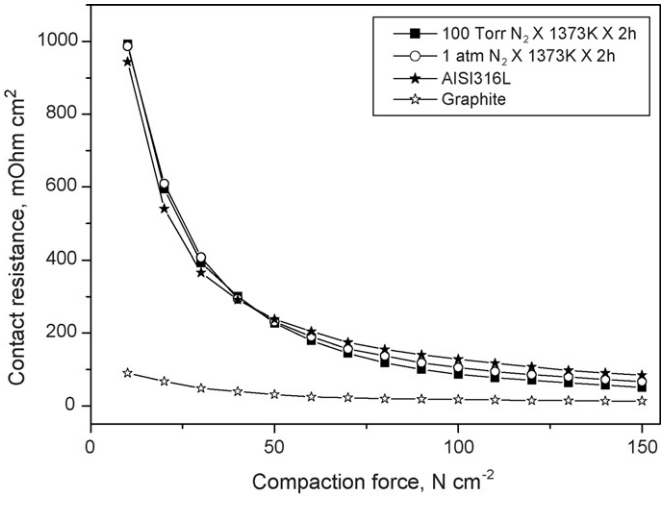

Fig. 6. Interfacial contact resistance of chromium nitrided AISI316L stainless steels as a function of compaction force. The results for AISI316L stainless steel and graphite are added for comparison.

the differences in the surface roughness of the nitride and bare stainless steels. The effect of the compaction force may be greater for a rough surface. The ICR values of the specimens nitrided at a nitrogen pressure of 100 Torr are lower than those of the specimens nitrided at 1 atm for all packing loads. The ICR values of the specimens nitrided at 100 Torr and 1 atm are 50 and 66 mΩ cm^2, respectively, at a compaction force of 150 N cm^{-2}. Higher ICR values are expected for the specimens nitrided at 1 atm based on the higher electrical resistivity of the top CrN layer.

3.4. Polarization curves

Potentiodynamic polarization curves for chromium nitride coated AISI316L stainless steel in 1 M H_2SO_4 + 2 ppm F^- solution at 80 °C are shown in Fig. 7. The polarization data for AISI316L stainless steel and graphite are also given for reference. Graphite is stable at an anode potential of −0.1 V and shows a corrosion current density of 1.81×10^{-6} A cm^{-2} at a cathode potential of 0.6 V. A corrosion current density of less than 1.6×10^{-5} A cm^{-2} is recommended for a bipolar plate [19] and is marked as a dashed line in Fig. 7. The corrosion current density of bare AISI316L stainless steel is higher than the recommended value, namely, 1.52×10^{-4} A cm^{-2} at the anode potential and 4.37×10^{-5} A cm^{-2} at the cathode potential. Both of the nitride coated steels show a lower corrosion current density than the recommended value. The corrosion current density of the Cr_2N nitride coated stainless steel is quite low at the initial potential (OCP) and is 5.87×10^{-7} A cm^{-2} at −0.1 V. As the potential is increased, the corrosion current density increases to 1.77×10^{-6} A cm^{-2} at 0.6 V, which is well below the recommended value and approaches the corrosion resistance of graphite. The corrosion current densities of the CrN + Cr_2N nitride coated stainless steel, viz., 4.99×10^{-6} A cm^{-2} and 8.61×10^{-6} A cm^{-2} at −0.1 V and 0.6 V, respectively, are higher than that of the single Cr_2N nitride coated steel.

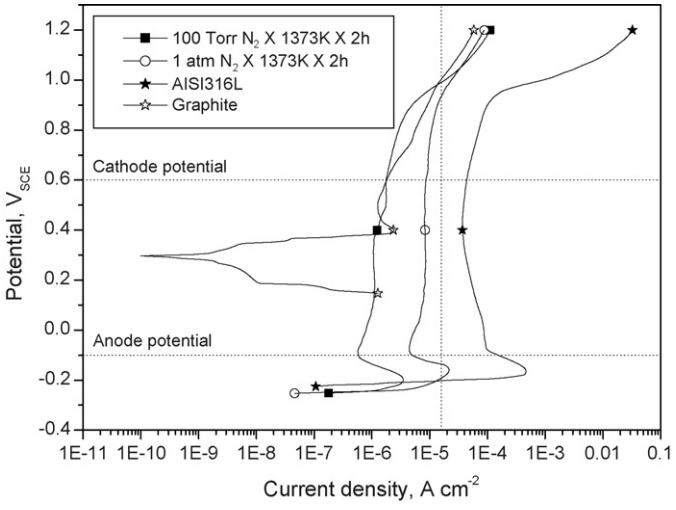

Fig. 7. Potentiodynamic curves for chromium nitrided AISI316L stainless steels in 1M H_2SO_4 + 2 ppm F^- at 80 °C and an RDE rotation speed of 500 rpm. The results for AISI316L stainless steel and graphite are added for comparison.

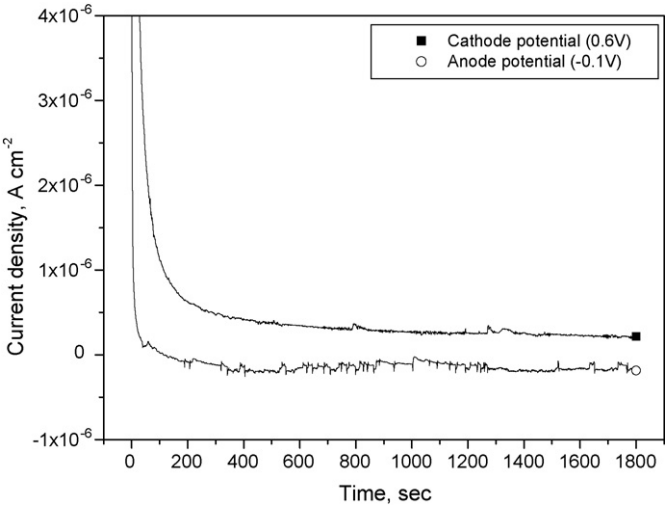

Fig. 8. Potentiostatic curves for 100 Torr N_2 nitrided AISI316L stainless steels in 1 M H_2SO_4 + 2 ppm F^- at 80 °C using an RDE at a rotation speed of 500 rpm.

The potentiostatic polarization test was performed to assess the stability of the chromium nitrided layer as a function of time. The potentiostatic polarization curves for the Cr_2N nitride coated AISI316L stainless steels at the anode and cathode potentials for 30 min are presented in Fig. 8. In all cases, the current densities fall sharply after the start of the polarization test and reach a stable steady-state. The current density at the anode potential shows an anodic current until about 2 min and then changes to a cathodic current, which is stable in the range of $(1–2) \times 10^{-7}$ A cm^{-2}. This means that the chromium nitrided layer hardly dissolves during the polarization test. The anodic current density at the cathode potential is in the rage of $(2–2.5) \times 10^{-7}$ A cm^{-2}.

The results of the potentiodynamic and potentiostatic polarization tests demonstrate that the thermally nitrided Cr_2N layer grown on chromium electroplated AISI316L stainless steels is very stable in a PEMFC corrosion environment and provides good corrosion resistance that is suitable for bipolar plates.

4. Discussion

Bipolar plates serve as blocking plates between the unit cells of the stack of the PEMFC, make electrical contact with the membrane electrode assembly (MEA), and transmit the electricity generated in the unit cell. Since the inside of the unit cell is a corrosive environment, the bipolar plate must have good corrosion resistance and the electrical resistivity of the surface of the plate which is in contact with the MEA should be low to enhance the electric efficiency of the cell. In addition, since several hundred bipolar plates are used in one fuel cell stack, the bipolar plate should be as thin as possible to make the entire stack compact.

At present, graphite or a carbon composite is generally used as the bipolar plate material for PEMFCs, and hydrogen and air pathways are formed in the bipolar plate by moulding or milling. Graphite bipolar plates have the advantages of good electrical conductivity and good corrosion resistance. Due to the high cost

of the graphite material itself and the high machining cost of the plate, however, the price of graphite bipolar plates is too high for their commercial application. In addition, due to their gragility, it is not easy to process graphite bipolar plates to a thickness of 4–5 mm or below. Thus, it is difficult to reduce the size of a fuel cell stack consisting of several tens to several hundreds of unit cells to a desirable dimension.

As an alternative to graphite/composite bipolar plate materials, many attempts have been made to use metal alloys. Metals have many properties required for the bipolar plate and have the advantages of low material and processing costs. On the other hand, metals can corrode in the oxidative environment inside the stack and oxide films that have a large electrical resistivity can easily form on the surface of the metallic bipolar plate. Problems such as membrane poisoning or an increase in contact resistance can also occur. Corrosion of a metallic bipolar plate can cause the formation of defects and poisoning and the catalyst and electrolyte due to the diffusion of metallic ions into the electrolyte membrane. When the catalyst is poisoned, its activity is degraded and when the electrolyte is poisoned, its ion conductivity deteriorates. In such cases, the performance of the fuel cell will also be degraded. In addition, because the corroded metal is in contact with the MEA, the ICR increases and the performance of the fuel cell will be further aggravated.

The corrosion problem represents the main obstacle to the application of metallic bipolar plates in fuel cells. In order to improve their corrosion resistance and reduce their contact resistance, surface modification of metal plates has been attempted. Such surface treatment includes the formation of a protective film on the surface of the base metal plate [7,20].

Among the several coatings that have been tried, chromium nitride coatings on high chromium alloy steels have been reported to be the most promising [7]. The cost of high-chromium alloy steels is still quite high, however, and the corrosion resistance of the coated layer is insufficient for fuel cells. The chromium nitrided layers formed on high-chromium steels have been found to contain two types of nitride, namely CrN and Cr_2N. The CrN layers forms first and the Cr_2N layers forms below the CrN layer. The CrN layer limits the nitrogen diffusion through the CrN layer and columnar growth of a Cr-rich Cr_2N layer below the CrN layer has been observed [21]. The electrical resistivity of CrN is very high, viz., 600–800 $\mu\Omega$ cm, which is about 7 to 10 times higher than that of Cr_2N, viz., 79–89 $\mu\Omega$ cm. In addition, due to the limited diffusion of nitrogen through CrN nitride, growth of Cr_2N layer is very sluggish and the π-phase forms below the Cr_2N layer [22]. In such a case, further growth of the Cr_2N layer will be hindered and the thickness of the protective chromium nitrided layer will be limited by this process. It is very desirable to form a Cr_2N layer only on the surface of the bipolar plate.

In this study, the thermal nitridation of an electroplated chromium layer on AISI316L stainless steel has been attempted. The nitridation condition was selected so as to form Cr_2N nitride only, and uniform growth of the Cr_2N layer was possible under these conditions (Figs. 4 and 5). The thickness of the Cr_2N layer is very much dependent on the thickness of the Cr electroplated layer but, due to the diffusion of iron into the Cr electroplated layer, an internal nitridation layer is observed to form below the uniform Cr_2N layer. Micro-voids are observed in the continuous Cr_2N layer, which are believe to form because of the volume contraction of electroplated amorphous Cr during heating. These voids are isolated and may not seriously affect the corrosion or electrical resistance of the nitrided layer.

The corrosion resistance of the Cr_2N layer, as evaluated by potentiodynamic polarization in 1 M H_2SO_4 + 2 ppm F^- solution at 80 °C, is very promising. Under the present experimental conditions, the corrosion current density of the Cr_2N layer, viz., 1.77×10^{-6} A cm^{-2} at 0.6 V, is an order of magnitude lower than that of the recommended value of 1.6×10^{-5} A cm^{-2} [19], and approaches the value of graphite, viz., 1.81×10^{-6} A cm^{-2}. The ICR of the Cr_2N layer, 50 mΩ cm^{-2} at 150 N cm^{-2}, is lower than those of AISI316 stainless steel and the CrN/Cr_2N layer. This value is about four times higher than that of graphite. Some improvements may be possible if the internal quality and surface roughness of the nitrided layer can be enhanced. A close transmission electron microscopical investigation of the defects in the nitrided layer is currently in progress.

5. Conclusions

Cr_2N chromium nitrided layers have been thermally grown on chromium electroplated AISI316L stainless steels and their use as a protective coating for metallic bipolar plates in a PEMFC stack has been evaluated. The conditions for the growth of nitride from the electroplated chromium layer are thermodynamically evaluated and are successfully applied to the growth of a uniform and continuous Cr_2N layer on the surface of stainless steel. The ICR of the Cr_2N layer is an order of magnitude lower than that of bare AISI316L stainless steel, and is also lower than that of the CrN + Cr_2N layer grown by the conventional nitriding condition at a nitrogen gas pressure of 1 atm. Potentiodynamic polarization curves show that the Cr_2N layer has better corrosion resistance than the CrN + Cr_2N layer, and that the current density at the cathode potential is similar to that of graphite. The Cr_2N layer grown by thermal nitridation of the electroplated chromium layer exhibits good interfacial contact and corrosion resistance and demonstrates excellent potential to be used as a protective coating layer for the bipolar plate of a PEMFC.

References

[1] EGG Services, Fuel Cell Handbook, 5th ed., U.S. Department of Energy, Morgatown, 2000, p. 1–1.
[2] H. Tsuchiya, O. Kobayashi, Int. J. Hydrogen Energy 29 (2004) 985.
[3] H. Wang, M.A. Sweikart, J.A. Turner, J. Power Sources 115 (2003) 243.
[4] M.P. Brady, K. Weisbrod, I. Paulauskas, R.A. Buchanan, K.L. More, H. Wang, M. Wilson, F. Garzon, L.R. Walker, Scripta Materialia 50 (2004) 1017.
[5] H. Wang, M.P. Brady, G. Teeter, J.A. Turner, J. Power Sources 138 (2004) 86.
[6] H. Wang, M.P. Brady, K.L. More, H.M. Meyer III, J.A. Turner, J. Power Sources 138 (2004) 79.
[7] M.P. Brady, B. Yang, H. Wang, J.A. Turner, K.L. More, M. Wilson, F. Garzon, JOM 58 (2006) 50.
[8] E. Menthe, K.-T. Rie, Surf. Coat. Technol. 112 (1999) 217.
[9] I. Masaru, J. Korean Soc. Heat Treat. 14 (2001) 179.

[10] J.K. Dennis, T.E. Such, Nickel and Chromium Plating, Butterworth, London, 1972, p. 186.
[11] M.W. Chase Jr., C.A. Davies, J.R. Downey Jr., D.J. Frurip, R.A. McDonald, A.N. Syverud, JANAF Thermochemical Tables, 3rd ed., The American Chemical Society and the American Institute of Physics for the National Bureau of Standards, Midland, 1985, pp. 934–939.
[12] Thermo-Calc Version Q, SUB97, Foundation for Computational Thermodynamics (2000).
[13] D.P. Davies, P.L. Adcock, M. Turpin, S.J. Rowen, J. Appl. Electrochem. 30 (2000) 101.
[14] D. Chu, R. Jiang, J. Power Sources 80 (1999) 226.
[15] R.L. Borup, N.E. Vanderborgh, Materials Research Society Symposium Proceedings Vol. 393, Materials Research Society, Pittsburgh, 1995, pp. 151–156.
[16] P.K. Ajkumar, A. Sankaran, M. Kamruddin, R. Nithya, P. Shankar, S. Dash, A.K. Tyagi, B. Raj, Surf. Coat. Technol 201 (2006) 102.
[17] W. Mayr, W. Lengauer, P. Ettmayer, D. Rafaja, J. Bauer, M. Bohn, J. Phase Equilibr. 20 (1999) 35.
[18] PCPDFWIN Version 1.30, Card Number 35-0803, JCPDS International Centre for Diffraction Data, 1997.
[19] J.S. Cooper, J. Power Sources 129 (2004) 152.
[20] H. Tawfik, Y. Hung, D. Mahajan, J. Power Sources 163 (2007) 755.
[21] M.P. Brady, K. Weisbrod, I. Paulauskas, R.A. Buchanan, K.L. More, H. Wang, M. Wilson, F. Garzon, L.R. Walker, Scripta Mater. 50 (2004) 1017.
[22] I.E. Paulauskas, M.P. Brady, H.M. Meyer III, R.A. Buchanan, L.R. Walker, Corros. Sci. 48 (2006) 3157.